PCCP

Accepted Manuscript

ROYAL SOCIETY OF CHEMISTRY

www.rsc.org/pccp

Cite this: DOI: 10.1039/c0xx00000x

www.rsc.org/xxxxxx

ARTICLE TYPE

Advanced thermoelectrics governed by single parabolic band: $Mg_2Si_{0.3}Sn_{0.7}$, a canonical example

Wei Liu,[a,b]† Hang Chi,[a]† Hui Sun,[a] Qiang Zhang,[b] Kang Yin,[b] Xinfeng Tang,*[b] Qingjie Zhang[b] and Ctirad Uher*[a]

Received (in XXX, XXX) Xth XXXXXXXXX 20XX, Accepted Xth XXXXXXXXX 20XX
DOI: 10.1039/b000000x

The well-known single parabolic band (SPB) model has been useful in providing insights into the understanding of transport properties of numerous thermoelectric materials. However, the conduction and valence bands of real semiconductors are rarely truly parabolic which limits the predictive power of the SPB model. The coincidence of the band edges of two parabolic bands, a situation arising in $Mg_2Si_{1-x}Sn_x$ solids solutions when $x \sim 0.7$, naturally makes applicable the SPB approximation to evaluate all transport parameters. We demonstrate this on the case of Bi-doped $Mg_2Si_{0.3}Sn_{0.7}$ where the minima of the two conduction bands at the X-point of the Brillouin zone coincide. The combination of a large density-of-states effective mass $m^* \sim 2.6\ m_e$ arising from the enhanced valley degeneracy N_v, high mobility μ_d due to low deformation potential E_d (8.77-9.43 eV), and ultra-low alloy scattering parameter E_a (0.32-0.39 eV) leads to an outstanding power factor, $PF_{max} \propto (m^*)^{3/2}\mu_d$, of up to 4.7 mW m^{-1} K^{-2} around 600 K. The specification and improved understanding of scattering parameters using the SPB model are important and instructive for further optimization of the thermoelectric performance of n-type $Mg_2Si_{0.3}Sn_{0.7}$.

Broader context

Thermoelectric materials can recover waste industrial heat (such as generated by cars and trucks) and convert it to electricity as well as provide efficient local cooling of electronic devices. Such purely solid state energy conversion assures not only an exceptionally reliable operation but also an environmentally responsible technological approach. Unlike the currently most highly developed thermoelectric materials based on PbTe and $Bi_{2-x}Sb_xTe_3$ that use expensive (Te) and environmentally harmful (Pb) chemical elements, $Mg_2Si_{1-x}Sn_x$ - based solid solutions are prepared from inexpensive, earth-abundant, and environmentally harmless raw materials. Their low density and promising thermoelectric performance bode well for large scale commercial applications. In this work we show that the excellent electronic properties (the power factor reaching 4.7 mW m^{-1} K^{-2}) of n-type Bi-doped $Mg_2Si_{0.3}Sn_{0.7}$ come from the increased valley degeneracy and enhanced density-of-states effective mass that is augmented by the low deformation potential and alloy scattering parameter. The convergence of the two parabolic conduction bands in the $Mg_2Si_{0.3}Sn_{0.7}$ band structure plays a pivotal role in this process and impels the use of the ***Single Parabolic Band*** model to accurately predict the thermoelectric performance of this material. Primarily due to its outstanding power factor, Bi-doped $Mg_2Si_{0.3}Sn_{0.7}$ achieves the highest dimensionless figure of merit ZT of 1.3 at around 700 K.

Main Text

Efficiency of a thermoelectric material is evaluated based on its dimensionless figure of merit defined as $ZT = S^2\sigma T/\kappa$, where S is the Seebeck coefficient, σ is the electrical conductivity, κ is the thermal conductivity, and T is the absolute temperature. Since transport parameters are interdependent, it is a challenging task to maximize the figure of merit. In the theoretical evaluation of transport properties, a variety of models are used, among them the most popular one is the single parabolic band (SPB) model.[1-3] Its appeal stems from its mathematical simplicity and readily available relevant formulae, offering an excellent initial evaluation of electronic properties of thermoelectric materials.[4-6] However, applying the SPB model in more quantitative studies often requires extra attention and care because the band structure of the existing materials is rarely strictly parabolic.

Among the most prospective novel thermoelectric systems[7, 8] are $Mg_2Si_{1-x}Sn_x$ solid solutions that are environmentally friendly, inexpensive, and do not contain harmful and scarce lead and tellurium. The coincidence of the two parabolic conduction band minima (CBM)[9-11] when $x = 0.7$ ($Mg_2Si_{0.3}Sn_{0.7}$), a situation rarely encountered in other promising thermoelectric material systems such as Bi_2Te_3,[12-15] PbTe,[4, 16, 17] skutterudite,[18-20] half Heusler compounds,[21, 22] and highly mismatched alloys,[23, 24] offers a unique opportunity to evaluate transport phenomena using the SPB model that should be rigorously applicable in this case. Forcing the SPB model on clearly non-parabolic band structures is unlikely to result in a meaningful agreement with experimental transport parameters, hence no useful predictive power can be expected. In this research, Bi-doped $Mg_2Si_{0.3}Sn_{0.7}$ solid solutions are adopted to evaluate the predictive power of the SPB model. In addition, the excellent electronic properties of $Mg_2(Si_{0.3}Sn_{0.7})_{1-y}Bi_y$, having the origin in the conduction band convergence,[10, 11]

are analyzed systematically.

$Mg_2(Si_{0.3}Sn_{0.7})_{1-y}Bi_y$ ($0 \le y \le 0.04$) solid solutions were prepared using high-purity elemental powders via a two-step solid state reaction (SSR) method[25, 26] (carried out at 873 K and 973 K for the first and second step, respectively), followed by a spark plasma sintering (SPS) process (at 953 K under the pressure of 30 MPa). An 8% Mg excess over its stoichiometric amount in $Mg_2Si_{0.3}Sn_{0.7}$ was chosen to compensate for the evaporation loss

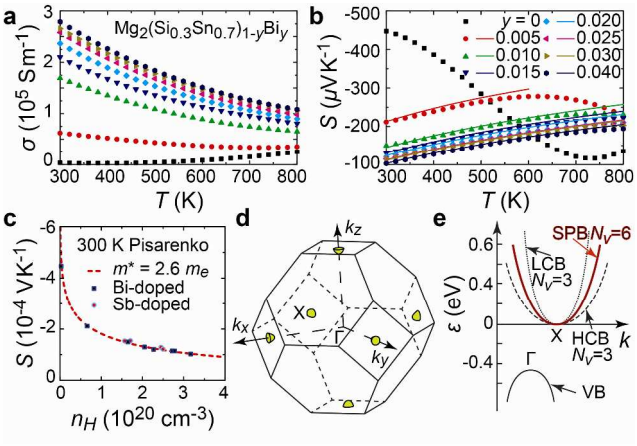

Fig. 1 Electronic properties of $Mg_2(Si_{0.3}Sn_{0.7})_{1-y}Bi_y$. (a) Temperature dependent electrical conductivity σ. (b) Experimental data (symbols) and theoretical results (lines) based on the single parabolic band (SPB) model for the Seebeck coefficient S. Excellent agreement between the data and the theory in the extrinsic range is evident. (c) The Pisarenko plot (S vs. Hall density n_H) at 300 K with a fixed density-of-states effective mass m^* reflects a single parabolic nature of the band structure invariant of doping and temperature (see Fig.1 b). (d) First Brillouin zone showing the three-fold degenerated (N_v = 3) electron pockets at X. (e) Schematic representation of the band structure (electron energy ε vs. wave vector k). The valence band (VB) is at Γ while the convergence of the light and heavy conduction bands (LCB and HCB) located at X point results in the doubled valley degeneracy (N_v = 6) at all temperatures of interest.

of Mg during the synthesis, as well as to offer an optimized carrier density and electrical performance. Ingots, following SPS processing, showed a very high density of nearly 99% of the theoretical value. These dense bulk ingots were then cut into suitable size for transport measurements. X-ray diffraction patterns of these solid solutions were measured on finely ground powders using a PANalytical X'Pert Pro type x-ray diffractometer with Cu Kα radiation. The actual composition was obtained from well-polished crystalline samples by a JXA-8230 SuperProbe Electron Probe Microanalyzer equipped with wavelength dispersive x-ray spectrometers (WDS). The electrical conductivity and the Seebeck coefficient in the range of 300-773 K were acquired on a commercial ZEM-1 apparatus (Ulvac Sinku-Riko) by a standard four-probe dc configuration. The thermal conductivity κ of samples above room temperature was obtained through the formula of $\kappa = \lambda C_p \rho$, where the thermal diffusivity λ was measured by the laser flash technique using a Netzsch LFA-457 instrument, the heat capacity at constant pressure C_p was obtained in a Q20 differential scanning calorimeter (TA Instruments), and the sample density ρ at room temperature was determined by the Archimedes' method. Differential scanning calorimetry (DSC) measurements were performed in the Q20 differential scanning calorimeter. The high temperature Hall coefficient was measured from 290 K to 780 K using a homemade Hall probe system in an oven inserted in a 9 T Oxford air-bore superconducting magnet. The data were recorded using a Linear Research AC Resistance Bridge (LR-700) operated with a 16 Hz excitation frequency at magnetic fields of ±1 T. Hall coefficient and electrical conductivity in the range of 10-300 K were obtained in a Quantum Design PPMS-9 system. The overall uncertainty of the electrical conductivity, the Seebeck coefficient and the thermal conductivity were estimated to be about ±3%, ±2% and ±5%, respectively. The room temperature longitudinal sound velocity v_l was measured by an ultrasonic pulse echo method (Panametrics 5072PR) with a fundamental frequency of 20 MHz.

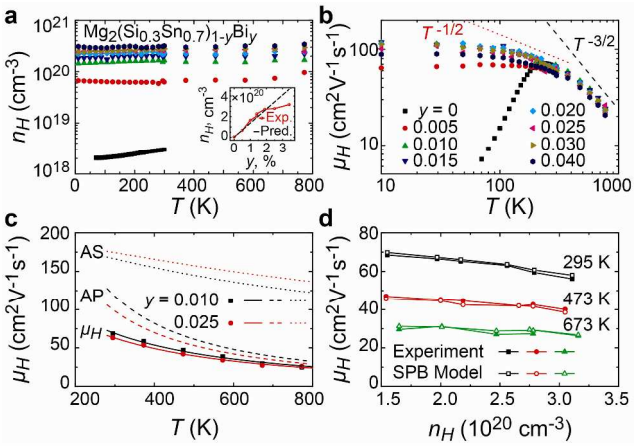

Fig. 2 Temperature dependent (a) Hall density n_H and (b) Hall mobility μ_H of $Mg_2(Si_{0.3}Sn_{0.7})_{1-y}Bi_y$ in the range of 10-773 K. The symbols in the inset of (a) illustrate the relationship between n_H and the actual Bi concentration, while the dashed line presents the theoretical prediction assuming that one Bi atom donates one electron to the structure. (c) The theoretical fitting of μ_H for the y = 0.010 and 0.025 samples indicates that acoustic phonon (AP) scattering dominates at high temperatures over alloy scattering (AS). (d) Plots of μ_H verse n_H at 295 K, 473 K and 673 K, respectively. The μ_H data show no significant deterioration upon increasing n_H, implying an excellent electronic performance.

The temperature dependent electrical conductivity σ of $Mg_2(Si_{0.3}Sn_{0.7})_{1-y}Bi_y$ ($0 \le y \le 0.04$) is shown in Fig. 1a. While the y = 0 sample behaves as a typical intrinsic semiconductor, Bi-doping drives the system into a highly degenerate semiconducting regime for $y \ge 0.010$, with the Hall density n_H on the order of 10^{20} cm^{-3} (see Table 1 and Fig. 2a). As shown in Fig. 1b and Table 1, the gradually decreasing magnitude of the Seebeck coefficient S with the increasing content of Bi maps well with the evolution of σ, reflecting the movement of the Fermi level E_F well into the conduction band (CB).

In the SPB model, all galvanomagnetic transport coefficients can be obtained (see Supplementary) assuming an energy dependent relaxation time $\tau = \tau_0 \varepsilon^r$. The calculated m^* at 300 K using a combination of the experimental S and n_H have shown little variation among the samples (see Table 1). The y = 0 sample is understandably different as a result of its intrinsic transport nature. As illustrated in Fig. 1c at 300 K, all Bi-doped samples (and also Sb-doped n-type $Mg_2Si_{0.3}Sn_{0.7}$) have fallen on the same Pisarenko line calculated using a fixed m^* (= 2.6 m_e), which confirms that the converged CBs can be viewed as a doubly degenerate SPB with N_v = 6 (see Fig. 1d and 1e).

Furthermore, the temperature dependence of S (lines in Fig. 1b) predicted using the fixed room temperature value of the density-of-states effective mass m^* (= 2.6 m_e) shows an excellent

agreement with the experimental data at all temperatures. The deviations at the highest temperatures between the data and the SPB model are the consequence of the onset of intrinsic excitations. The essentially constant value of m^* at all temperatures and carrier densities verifies that the SPB model truly captures the key features of the CBs and can be used to characterize and predict all transport properties of *n*-type $Mg_2Si_{0.3}Sn_{0.7}$ solid solutions.

Table 1 Transport parameters of $Mg_2(Si_{0.3}Sn_{0.7})_{1-y}Bi_y$ ($0 \le y \le 0.04$) at 300 K: Seebeck coefficient S (μV K^{-1}), Hall density n_H (10^{20} cm^{-3}), Hall mobility μ_H (cm^2 V^{-1} s^{-1}), reduced Fermi level η (= E_F/k_BT), Hall factor r_H, and the density-of-states effective mass m^* (in units of the electron rest mass m_e).

y	Actual Composition	S	n_H	μ_H	η	r_H	m^*
0	$Mg_{2.10}Si_{0.29}Sn_{0.71}$	-447	0.03	64	-3.17	1.18	2.25
0.005	$Mg_{2.09}Si_{0.29}Sn_{0.71}Bi_{0.005}$	-211	0.66	59	-0.10	1.14	2.62
0.010	$Mg_{2.12}Si_{0.28}Sn_{0.71}Bi_{0.010}$	-150	1.65	58	1.03	1.10	2.74
0.015	$Mg_{2.08}Si_{0.26}Sn_{0.73}Bi_{0.014}$	-130	2.05	61	1.50	1.09	2.58
0.020	$Mg_{2.08}Si_{0.28}Sn_{0.70}Bi_{0.014}$	-120	2.27	64	1.76	1.08	2.49
0.025	$Mg_{2.07}Si_{0.28}Sn_{0.70}Bi_{0.019}$	-115	2.72	57	1.93	1.08	2.64
0.030	$Mg_{2.10}Si_{0.24}Sn_{0.73}Bi_{0.025}$	-114	2.78	60	1.94	1.08	2.67
0.040	$Mg_{2.07}Si_{0.25}Sn_{0.71}Bi_{0.034}$	-103	3.17	53	2.33	1.07	2.54

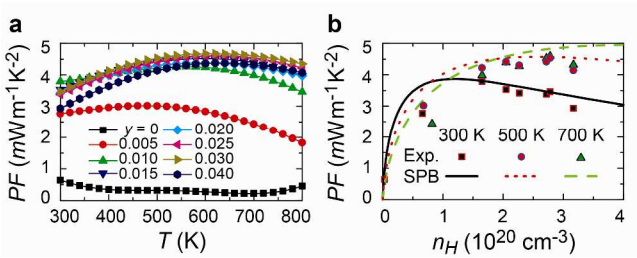

Fig. 3 (a) Temperature dependent power factor (PF) of $Mg_2(Si_{0.3}Sn_{0.7})_{1-y}Bi_y$. (b) The predicted PF based on the single parabolic band (SPB) model, in agreement with the experimental data.

The SPB nature of the *n*-type $Mg_2Si_{0.3}Sn_{0.7}$ thus offers a canonical testing ground for the transport study, which has rarely been so neatly accessible elsewhere. The carrier density as a function of Bi doping is depicted in Fig. 2a. A rather weak temperature dependence of the carrier density attests to a highly degenerate semiconductor. At low doping levels, see the inset in Fig. 2a, Bi is a single electron donor, specifically when the actual Bi content y is lower than 0.02. However, the doping efficiency of Bi drops down rapidly with the further increase of Bi content which is associated with the limited solubility of Bi, indirectly confirmed by the indistinct lattice thermal conductivity κ_L for $y \ge 0.020$, seen in Fig. 4b. As shown in Fig. 2b, at high temperatures, acoustic phonons (AP) dominate the transport behavior, leading to a temperature dependence of $\mu_H^{AP} \propto T^{-3/2}$, while around ambient temperatures, alloy scattering (AS, $\mu_H^{AS} \propto T^{-1/2}$) appears to contribute relatively more significantly to the overall μ_H.[27] Indeed, as illustrated in Fig. 2c, typical weight of acoustic phonon scattering defined as $\Omega^{AP} = (1/\mu_H^{AP})/(1/\mu_H)$ has increased from ~ 60% at 295 K to ~ 80% at 673 K. The μ_H can be decomposed into its chief components (AP and AS) via the Matthiessen's rule:[28]

$$\frac{1}{\mu_H} = \frac{1}{\mu_H^{AP}} + \frac{1}{\mu_H^{AS}}. \qquad (1)$$

The mobility appropriate for acoustic phonon scattering is given by[29]

$$\mu_H^{AP} = \frac{(8\pi)^{1/2} e\hbar^4 \rho v_l^2}{3E_d^2 (m_s^*)^{5/2} (k_B T)^{3/2}} \Psi_r(\eta), \qquad (2)$$

where e is the elementary charge, $\hbar$ is the reduced Planck constant, k_B is the Boltzmann constant, ρ is the density, v_l (5.29×10^3 m s^{-1}) is the longitudinal velocity of sound, and E_d is the deformation potential describing the strength of the electron-phonon interaction. The single valley effective mass m_s^* is related to m^* via $m^* = N_v^{2/3} m_s^*$. Regarding alloy scattering, the relevant formula for the mobility is[30]

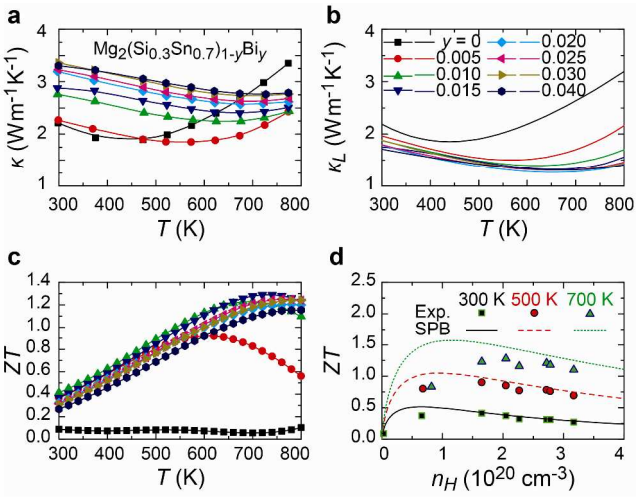

Fig. 4 Temperature dependent (a) thermal conductivity κ, (b) lattice thermal conductivity κ_L and (c) dimensionless figure of merit ZT of $Mg_2(Si_{0.3}Sn_{0.7})_{1-y}Bi_y$. (d) The predicted ZT based on the SPB model (lines) are in accord with the experimentally determined ZT (symbols). Note the significant bipolar effect at elevated temperatures, especially for samples with low doping levels.

$$\mu_H^{AS} = \frac{64e\hbar^4 N_0}{9(2\pi)^{3/2} x(1-x) E_a^2 (m_s^*)^{5/2} (k_B T)^{1/2}} \Psi_r(\eta), \qquad (3)$$

where N_0 is the number of atoms per unit volume, x (= 0.7) is the Sn fraction in the solid solution of $Mg_2Si_{0.3}Sn_{0.7}$, and E_a is the parameter characterizing the alloy potential fluctuation. The common factor $\Psi_r(\eta)$ is a scattering-mechanism-specific term (Supplementary Eq. S10) determined by the reduced Fermi level η (= E_F/k_BT) through a combination of the Hall factor r_H and Fermi-Dirac integrals $F_n(\eta)$ and is taken to be identical for both AP and AS scattering processes (r = -1/2 as the mean-free path is assumed energy independent in both cases[31]).

According to Eq. 2 and Eq. 3, μ_H^{AP} and μ_H^{AS} have a similar dependence on m_s^* and the characteristic potentials E_d and E_a. Fitting of μ_H vs. T for our *n*-type $Mg_2Si_{0.3}Sn_{0.7}$ samples indicates (see Fig. 2c and 2d) that the model including μ_H^{AP} and μ_H^{AS} quantitatively characterizes the experimental μ_H and its temperature dependence. The values of E_d (8.77-9.43 eV) and E_a (0.32-0.39 eV) were then obtained. Literature values for potentials E_d and E_a for a range of semiconductors including n-type $Mg_2Si_{1-x}Sn_x$[32,33], the III-V compounds[34-37], n-type $Si_{1-x}Ge_x$[38], n-type PbS[27], $PbSe_{1-x}Te_x$[39,40], and n-type $Cd_{1-x}Zn_xTe$[41] are in the range of 5-35 eV and 0.6-2.0 eV, respectively. While the parameter E_d of our *n*-type $Mg_2Si_{0.3}Sn_{0.7}$ is comparable to the

lowest reported values, the alloy fluctuation parameter E_a is apparently much smaller than the reported literature values. Although our *n*-type $Mg_2Si_{0.3}Sn_{0.7}$ possesses a much larger m_s^* (≈ 0.79 m_e) compared to the effective mass (0.07-0.60 m_e) for most of the above mentioned semiconductors, its reasonably large room temperature mobility of ~ 60 $cm^2 V^{-1} s^{-1}$ is primarily due to the weak electron-phonon interaction (low E_d) and the rather limited effect on the mobility from the alloy disorder (ultra-low E_a). According to Brooks[30,38], the parameter E_a evaluates potential fluctuation in alloys caused by the alloy disorder, which is generally believed to be related to the band gap difference ΔE_g or the band edge difference (or the electron affinity difference $\Delta\chi$ in *n*-type materials) between the two end members in the alloy series. However, there are semiconductors such as the III-V compounds, *n*-type $Si_{1-x}Ge_x$ and *n*-type $Cd_{1-x}Zn_xTe$ where the discrepancy between E_a and ΔE_g ($\Delta\chi$) is large, probably due to the fact that the band edges of these semiconductors do not have strictly the SPB character. In our research, the values of E_a (0.32-0.39eV) for *n*-type $Mg_2Si_{0.3}Sn_{0.7}$ are quite comparable to ΔE_g (~ 0.42 eV),[8-10] and/or $\Delta\chi$ (~ 0.19 eV)[42, 43] between Mg_2Si and Mg_2Sn. We ascribe such good agreement between E_a and ΔE_g ($\Delta\chi$) to the fact that the electronic transport is very precisely described by the SPB model in the entire temperature range investigated. Roughly twice the value of E_a (~ 0.7 eV) reported for $Mg_2Si_{0.45}Sn_{0.55}$ in the Ref. 33 should be attributed to a non-uniform distribution of Si/Sn atoms (and thus extra scattering among different phases) as this composition falls in the range of the miscibility gap of the pseudo-binary phase diagram of Mg_2Si-Mg_2Sn.[8,26,44] Moreover, a contributing factor to the low value of E_a in our *n*-type $Mg_2Si_{0.3}Sn_{0.7}$ is a zero band offset between the light and heavy conduction bands (band convergence) while $Mg_2Si_{0.45}Sn_{0.55}$ has a finite offset (~ 0.1 eV) that may result in a certain amount of interband scattering.[9, 10]

Thus, low values of E_d and E_a, as well as the high Seebeck coefficient due to the conduction band convergence, lead to an outstanding power factor in $Mg_2(Si_{0.3}Sn_{0.7})_{1-y}Bi_y$ above 400 K, where values as high as 4.7 mW m^{-1} K^{-2} have been recorded for carrier concentrations of $2.05\times10^{20} \le n_H \le 2.78\times10^{20}$ cm^{-3}, as shown in Fig. 3a. Figure 3b displays plots of PF vs. n_H calculated based on the SPB model at typical temperatures of 300 K, 500 K and 700 K. The agreement with the experimental data is good and even improves at high n_H above 1.65×10^{20} cm^{-3}, where the bipolar contribution interferes less with the data.

The temperature dependent thermal conductivity κ and the lattice thermal conductivity κ_L (obtained by subtracting $\kappa_e = L\sigma T$ from κ using the Wiedemann-Franz law, where L is the Lorenz number) are shown in Fig. 4a and 4b, respectively. The κ_L derived in this way inevitably includes a contribution from the bipolar thermal conductivity κ_b at high temperatures (sharp upturn on both κ and κ_L). The κ_e amounts for a large fraction of the total thermal conductivity as well as for its dependence upon doping by Bi. Bi-doping significantly decreases the κ_L via strengthened point defect phonon scattering. This trend continues for samples with Bi content up to 0.02 at which point the lattice thermal conductivity of solid solutions becomes independent of the content of Bi. This reflects the limited ~ 2% solubility of Bi in the matrix. The lattice thermal conductivity κ_L exhibits a nearly $T^{-0.5}$ temperature dependence for all samples before the bipolar contribution κ_b becomes significant. The deviation from the classical T^{-1} dependence, expected from the usual phonon Umklapp interactions, indicates that point defects scattering still plays an important role in shaping the temperature profile of κ_L at high temperatures.[45] The ultimate value of ZT (= $S^2\sigma T/\kappa$) of $Mg_2(Si_{0.3}Sn_{0.7})_{1-y}Bi_y$ ~ 1.3 is limited by the intrinsic excitation processes which make a notable contribution above 700 K, see Fig. 4c. The averaged ZT value in the range of 300-800 K is ~ 0.9. As shown in Fig. 4d, the predicted ZT values (lines), calculated using the SPB model with κ_L being an experimental parameter, are in excellent agreement with experimental results, especially at 300 K and 500 K. Deviations observed at 700 K or in the low n_H region between the theory and the experiment are due to the interference of the bipolar effect which was not considered in the SPB model.

Thus, it has been established that *n*-type $Mg_2Si_{0.3}Sn_{0.7}$ can be regarded as a canonical example of the SPB model, a case rarely demonstrated in other material systems. The effort in determining the two key scattering parameters E_d and E_a, as well as the clear physical interpretation of the scattering process at and above room temperature, is important and instructive for enhancing the carrier mobility of this material in the future. Moreover, the attempt to suppress the bipolar effect and further reduce the κ_L through various routes, such as increasing the m^* of the valence band edge[2] and introducing *in-situ* formed nanostructures in the matrix of the bulk material,[17, 46-49] will be critical for further optimization of the figure of merit of *n*-type $Mg_2Si_{0.3}Sn_{0.7}$.

Conclusions

This research has shown that $Mg_2Si_{0.3}Sn_{0.7}$ with converged conduction bands is an excellent testing ground for the SPB model. It offers an opportunity to precisely characterize and account for all thermal and electronic transport properties of n-type $Mg_2Si_{0.3}Sn_{0.7}$. The experimental study and theoretical modelling of Bi-doped $Mg_2Si_{0.3}Sn_{0.7}$ have revealed that the enhanced m^* (due to doubled number of the carrier pockets N_v) together with the high μ_H (as a result of the low values of E_d and E_a) yield an outstanding PF and ZT of ~ 1.3 at 700 K. Small values of E_d of 8.77-9.43 eV in this work indicate that the electron-phonon coupling is weak in *n*-type $Mg_2Si_{0.3}Sn_{0.7}$. In addition, a small E_a of 0.32-0.39 eV in *n*-type $Mg_2Si_{1-x}Sn_x$ attests to its physical interpretation as being related to either the indirect band gap difference (~ 0.42 eV) or the electron affinity difference (~ 0.19 eV) between Mg_2Si and Mg_2Sn. Further improvements in ZTs of *n*-type $Mg_2Si_{0.3}Sn_{0.7}$ are expected to be achieved by suppressing the bipolar effect and reducing the lattice thermal conductivity.

Acknowledgements

We wish to acknowledge supports of the International Science & Technology Cooperation Program of China (Grant No. 2011DFB60150), the Natural Science Foundation of China (Grant No. 51172174), the 111 Project (Grant No. B07040). High temperature Hall effect measurements at U of M were carried out

with the support of CERC-CVC, the U.S.-China program supported by the U.S. Department of Energy under Award Number DE-PI0000012. The authors also would like to acknowledge Doctor Meijun Yang (from the Center for Materials Research and Analysis of Wuhan University of Technology) for the assistance on the EPMA measurements.

Notes and references

[a] *Department of Physics, University of Michigan, Ann Arbor, Michigan 48109, USA; E-mail: cuher@umich.edu*
[b] *State Key Laboratory of Advanced Technology for Materials Synthesis and Processing, Wuhan University of Technology, Wuhan 430070, China; E-mail: tangxf@whut.edu.cn*
† These authors contributed equally to this work.
‡ Electronic Supplementary Information (ESI) available: SPB model, XRD, DSC, and additional Pisarenko plots for $Mg_2Si_{1-x}Sn_x$. See DOI: 10.1039/b000000x/

1. H. J. Goldsmid, *Electronic Refrigeration*, Pion, London, 1986.
2. E. H. Putley, *The Hall Effect and Related Phenomena*, Butterworths, London, 1960.
3. G. J. Snyder and E. S. Toberer, *Nature Materials*, 2008, **7**, 105-114.
4. J. P. Heremans, V. Jovovic, E. S. Toberer, A. Saramat, K. Kurosaki, A. Charoenphakdee, S. Yamanaka and G. J. Snyder, *Science*, 2008, **321**, 554-557.
5. C. M. Jaworski, V. Kulbachinskii and J. P. Heremans, *Phys. Rev. B*, 2009, **80**, 233201.
6. Q. Zhang, B. Liao, Y. Lan, K. Lukas, W. Liu, K. Esfarjani, C. Opeil, D. Broido, G. Chen and Z. Ren, *Proceedings of the National Academy of Sciences*, 2013, **110**, 13261-13266.
7. D. M. Rowe, ed., *CRC Handbook of Thermoelectrics*, CRC Press, Boca Raton, FL, 1995.
8. D. M. Rowe, ed., *Thermoelectrics Handbook: Macro to Nano*, CRC Press, Boca Raton, FL, 2006.
9. V. K. Zaitsev, M. I. Fedorov, E. A. Gurieva, I. S. Eremin, P. P. Konstantinov, A. Y. Samunin and M. V. Vedernikov, *Phys. Rev. B*, 2006, **74**, 045207.
10. W. Liu, X. Tan, K. Yin, H. Liu, X. Tang, J. Shi, Q. Zhang and C. Uher, *Phys. Rev. Lett.*, 2012, **108**, 166601.
11. K. Kutorasiński, J. Tobola and S. Kaprzyk, *Phys. Rev. B*, 2013, **87**, 195205.
12. H. Chi, W. Liu, K. Sun, X. Su, G. Wang, P. Lošťák, V. Kucek, Č. Drašar and C. Uher, *Phys. Rev. B*, 2013, **88**, 045202.
13. B. Poudel, Q. Hao, Y. Ma, Y. Lan, A. Minnich, B. Yu, X. Yan, D. Wang, A. Muto, D. Vashaee, X. Chen, J. Liu, M. S. Dresselhaus, G. Chen and Z. Ren, *Science*, 2008, **320**, 634-638.
14. W. Xie, J. He, H. J. Kang, X. Tang, S. Zhu, M. Laver, S. Wang, J. R. D. Copley, C. M. Brown, Q. Zhang and T. M. Tritt, *Nano Lett*, 2010, **10**, 3283-3289.
15. R. J. Mehta, Y. Zhang, C. Karthik, B. Singh, R. W. Siegel, T. Borca-Tasciuc and G. Ramanath, *Nat Mater*, 2012, **11**, 233-240.
16. Y. Z. Pei, X. Y. Shi, A. LaLonde, H. Wang, L. D. Chen and G. J. Snyder, *Nature*, 2011, **473**, 66-69.
17. K. Biswas, J. He, I. D. Blum, C.-I. Wu, T. P. Hogan, D. N. Seidman, V. P. Dravid and M. G. Kanatzidis, *Nature*, 2012, **489**, 414-418.
18. C. Uher, in *Recent Trends in Thermoelectric Materials Research I*, ed. T. M. Tritt, Academic Press Inc, San Diego, 2001, vol. 69, pp. 139-253.
19. M. M. Koza, M. R. Johnson, R. Viennois, H. Mutka, L. Girard and D. Ravot, *Nature Mater.*, 2008, **7**, 805-810.
20. X. Shi, J. Yang, J. R. Salvador, M. Chi, J. Y. Cho, H. Wang, S. Bai, J. Yang, W. Zhang and L. Chen, *J. Am. Chem. Soc.*, 2011, **133**, 7837-7846.
21. C. Uher, J. Yang, S. Hu, D. T. Morelli and G. P. Meisner, *Phys. Rev. B*, 1999, **59**, 8615-8621.
22. Y. Liu, P. Sahoo, J. P. A. Makongo, X. Zhou, S.-J. Kim, H. Chi, C. Uher, X. Pan and P. F. P. Poudeu, *J. Am. Chem. Soc.*, 2013, **135**, 7486-7495.
23. J.-H. Lee, J. Wu and J. C. Grossman, *Phys. Rev. Lett.*, 2010, **104**, 016602.
24. H. Chi, C. Chen, J. D. Phillips and C. Uher, *Appl. Phys. Lett.*, 2013, **103**, 042108-042105.
25. W. Liu, X. Tang, H. Li, J. Sharp, X. Zhou and C. Uher, *Chem. Mater.*, 2011, **23**, 5256-5263.
26. W. Liu, X. Tang, H. Li, K. Yin, J. Sharp, X. Zhou and C. Uher, *J. Mater. Chem.*, 2012, **22**, 13653-13661.
27. Y. I. Ravich, B. A. Efimova and I. A. Smirnov, *Semiconducting Lead Chalcogenides*, Plenum Press, New York, 1970.
28. M. Kaviany, *Heat Transfer Physics*, Cambridge, New York, 2008.
29. J. Bardeen and W. Shockley, *Phys. Rev.*, 1950, **80**, 72-80.
30. J. W. Harrison and J. R. Hauser, *Phys. Rev. B*, 1976, **13**, 5347-5350.
31. V. I. Fistul', *Heavily Doped Semiconductors*, Plenum Press, New York, 1969.
32. L. D. Crossman and G. C. Danielson, *Phys. Rev.*, 1968, **171**, 867-875.
33. X. Liu, T. Zhu, H. Wang, L. Hu, H. Xie, G. Jiang, G. J. Snyder and X. Zhao, *Adv. Energy Mater.*, 2013, **3**, 1238-1244.
34. A. Chandra and L. F. Eastman, *J. Appl. Phys.*, 1980, **51**, 2669-2677.
35. D. C. Look, D. K. Lorance, J. R. Sizelove, C. E. Stutz, K. R. Evans and D. W. Whitson, *J. Appl. Phys.*, 1992, **71**, 260-266.
36. E. Bellotti, F. Bertazzi and M. Goano, *J. Appl. Phys.*, 2007, **101**, -.
37. V. W. L. Chin, *J. Phys. Chem. Solids*, 1991, **52**, 1193-1195.
38. S. Krishnamurthy, A. Sher and A.-B. Chen, *Appl. Phys. Lett.*, 1985, **47**, 160-162.
39. H. Wang, Y. Pei, A. D. LaLonde and G. J. Snyder, *Proceedings of the National Academy of Sciences*, 2012, **109**, 9705-9709.
40. H. Wang, A. D. LaLonde, Y. Pei and G. J. Snyder, *Adv. Funct. Mater.*, 2013, **23**, 1586-1596.
41. D. Chattopadhyay, *Solid State Communications*, 1994, **91**, 149-151.
42. A. Atanassov and M. Baleva, *Thin Solid Films*, 2007, **515**, 3046-3051.
43. M. Schoijet, *Solar Energy Materials*, 1979, **1**, 43-57.
44. I.-H. Jung, D.-H. Kang, W.-J. Park, N. J. Kim and S. Ahn, *Calphad*, 2007, **31**, 192-200.
45. T. M. Tritt, ed., *Thermal Conductivity Theory, Properties, and Applications*, Kluwer Academic / Plenum Publishers, New York, 2004.
46. L.-D. Zhao, S. Hao, S.-H. Lo, C.-I. Wu, X. Zhou, Y. Lee, H. Li, K. Biswas, T. P. Hogan, C. Uher, C. Wolverton, V. P. Dravid and M. G. Kanatzidis, *J. Am. Chem. Soc.*, 2013, **135**, 7364-7370.
47. L.-D. Zhao, S.-H. Lo, J. He, H. Li, K. Biswas, J. Androulakis, C.-I. Wu, T. P. Hogan, D.-Y. Chung, V. P. Dravid and M. G. Kanatzidis, *J. Am. Chem. Soc.*, 2011, **133**, 20476-20487.
48. L.-D. Zhao, J. He, C.-I. Wu, T. P. Hogan, X. Zhou, C. Uher, V. P. Dravid and M. G. Kanatzidis, *J. Am. Chem. Soc.*, 2012, **134**, 7902-7912.
49. L.-D. Zhao, J. He, S. Hao, C.-I. Wu, T. P. Hogan, C. Wolverton, V. P. Dravid and M. G. Kanatzidis, *J. Am. Chem. Soc.*, 2012, **134**, 16327-16336.

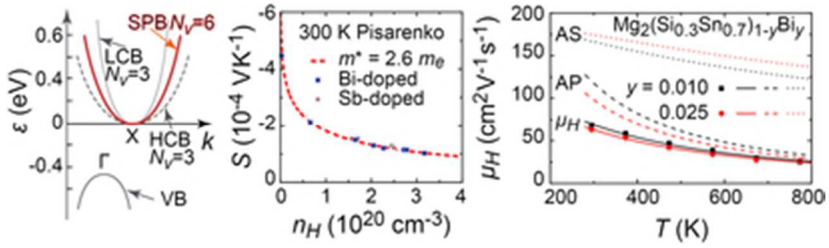

Enhanced thermoelectric performance of Bi-doped $Mg_2Si_{0.3}Sn_{0.7}$ with conduction band convergence has been successfully interpreted using the single parabolic (SPB) model. The improved understanding of scattering parameters is important and instructive for further optimization of n-type $Mg_2Si_{0.3}Sn_{0.7}$.
34x10mm (300 x 300 DPI)